Journal of
Materials Chemistry C

PAPER

View Article Online
View Journal | View Issue

Cite this: J. Mater. Chem. C, 2016, 4, 8429

Tunable optical properties of OH-functionalised graphene quantum dots†

K. R. Geethalakshmi,*[a] Teng Yong Ng[a] and Rachel Crespo-Otero*[b]

Received 4th July 2016,
Accepted 16th August 2016

DOI: 10.1039/c6tc02785g

www.rsc.org/MaterialsC

Graphene oxide quantum dots (**GO-QDs**) have distinct optoelectronic properties for their application in bio-imaging, drug delivery and photovoltaics. Herein, the effect of OH functionalisation on the optical properties of **GO-QDs** is studied based on state-of-the-art theoretical simulations. Our calculations predict the effect of OH groups on ionisation potentials, light absorption and emission properties. The mechanism of fluorescence is analysed considering the role of geometry distortion and charge transfer. Moreover, selective functionalisation of positions with large electron–hole separation offers a strategy to tune the optical gap and photoluminescence properties. These results open up new opportunities for the design of **GO-QDs** for a wide range of applications.

A. Introduction

Graphene oxide (GO) is evolving as a multifaceted candidate material for optoelectronics,[1] next-generation ultrathin electronics,[2,3] energy conversion and storage technologies.[4–6] However, the underlying issue currently limiting the direct attachment of GO to devices is the poor understanding of how to enforce spatial control over oxygen groups in the experimental processes.[7–9] These restrictions result in large optical gaps and drive poor electronic conductivity.[1,10,11]

GO has strong absorption in the ultraviolet region showing energy shifts towards the visible with increasing level of oxidation.[12,13] GO contains oxygen mainly in the form of epoxy, hydroxyl and carboxyl functional groups on the basal plane and at the sheet edges.[7,14] Hydroxyl groups stabilise the surface, help radiative recombination and consequently enhance the fluorescence yield.[15–17] Selective chemical reduction of carboxyl and epoxy groups with $NaBH_4$ increases the fraction of hydroxyl groups.[17]

The photoluminescence properties of GO can be tuned from deep ultraviolet to near infrared by reducing the size to the nanoscale regime and by controlling edge configuration effects, functional groups and defects.[18] These so-called graphene oxide quantum dots (**GO-QDs**) have received considerable attention because of their distinct structural and optoelectronic properties and for their potential application in fields such as bio-imaging, drug delivery and photovoltaics.[19,20]

Synthesis methods have not been very successful in producing **GO-QDs** with controllable size or functionalities and reaction conditions strongly affect the absorption and emission spectra.[19,21] **GO-QDs**, in the size range of 1–4 nm, were synthesised by Peng *et al.* and were demonstrated to show photoluminescence tunability.[22] The first absorption peak shifted from 330 to 270 nm when the temperature changed from 80 to 120 °C. Jang *et al.* synthesised **GO-QDs** with different amounts of oxygen using direct oxidation of graphite nanoparticles and by conventional chemical reduction.[19] **GO-QDs** of similar sizes obtained by different methods showed different carrier dynamics, but similar tendencies with regard to the oxygen composition.

In this context, the combined effects of oxygen content and size on the mechanisms of light absorption and luminescence are not well understood and inconsistent experimental outcomes have led to contradictory hypotheses due to large heterogeneity in the synthesised **GO-QDs**. There are two interpretations of the mechanism of fluorescence: localization of sp^2 clusters and involvement of oxygen functional groups. Herein, we analyse both mechanisms based on state-of-the-art theoretical simulations.[21]

Theoretical calculations are particularly useful to isolate the effect of different factors contributing to a particular mechanism. Several groups have explored the properties of graphene quantum dots (**G-QDs**) using different levels of theoretical approximations.[18,23–31] Recently, Yamijala *et al.* studied the nonlinear optical properties of **G-QDs** and found that QDs with zigzag edges show interesting optical properties.[32] The tunability of the emission of QDs has been recently analysed considering the effect of different functional groups.[18]

Herein, we evaluate the effect of the OH functionalisation on the ionisation potentials, absorption and emission properties of **GO-QD** zigzag edge models. Our results show a clear strategy

[a] School of Mechanical and Aerospace Engineering, Nanyang Technological University Singapore, 50 Nanyang Avenue, Singapore-639798. E-mail: geethalakshmikr@gmail.com
[b] School of Biological and Chemical Sciences, Materials Research Institute, Queen Mary University of London, Mile End Road, London E1 4NS, UK. E-mail: r.crespo-otero@qmul.ac.uk

† Electronic supplementary information (ESI) available. See DOI: 10.1039/c6tc02785g

to tune the properties of **GO-QDs** based on size and distribution of OH functional groups. These results contribute to a better understanding of their properties with implications for the design of more efficient **GO-QD** based devices.

B. Models and methods

We considered different functionalisation patterns and number of OH groups on small sized zigzag **GO-QDs**. The models were built by modifying the pristine QDs: coronene $C_{24}H_{12}$ (**G2**), ovalene, $C_{32}H_{14}$ (**G3**) and cir-coronene $C_{54}H_{18}$ (**G4**). Considering the general composition C_nH_m, we added 2, 4, m and m + 2 (**G2** and **G3**) or m + 4 (**G4**) OH groups. The OH groups were added forming bonds with carbon atoms from the basal plane and substituting the hydrogens of the edge planes. Symmetrical and non-symmetrical **GO-QDs** with respect to two C_2 symmetry axes were studied based on the functionalisation patterns shown in Fig. 1. Yan *et al.* showed that the most stable configurations contain epoxide and hydroxyl groups in close proximity.[16] We calculated models where the hydroxyl groups are relatively close, which stabilises the surface due to the formation of hydrogen bonds. All the considered models and their total energies are reported in the ESI.†

Functionalisation induces distortion of the geometry which affects the properties. Herein, distortion from planarity was measured by calculating the deviation of each ring from the plane. Considering the six possible dihedrals formed by the carbons connected by bonds, the maximum deviation from the plane was defined as the absolute value of the larger of these angles (θ_i). The average of these angles (θ) was used as a measure of geometric distortion (see the values for all the **GO-QDs** in the ESI†).

Theoretical methods are very useful to interpret the nature of electronic excitations, but the level of theory should be carefully chosen. A proper description of charge transfer (CT) states is very important for the analysis of the mechanism of fluorescence. It has been suggested that there is an important role of the functional groups in the fluorescence mechanism of **G-QDs**.[21] To study the electronic and optical properties of the **GO-QDs**, density functional theory (DFT) and linear response time-dependent functional theory (TDDFT)[33] calculations were performed.

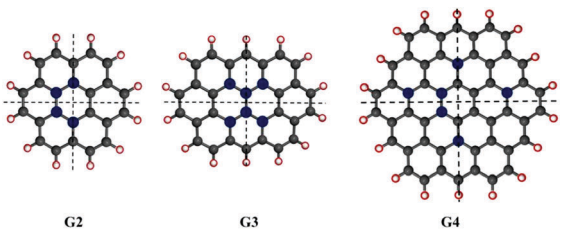

Fig. 1 Pristine graphene quantum dots considered in this study. The positions functionalised for the axial plane substitutions are shown in red, and the carbons that were functionalised with OH are shown in blue. The average radii of these QDs are 0.92 nm, 1.05 nm and 1.39 nm respectively.

Two density functionals were considered, the hybrid B3LYP[34] and the long-range corrected functional ωB97X-D.[35] It is well known that typical hybrid functionals, like B3LYP, have problems in describing CT states. B3LYP is still one of the most popular hybrid functionals and some of the previous calculations of quantum dots with a similar size have been performed with this functional.[18] These problems are alleviated using long-range corrected functionals like ωB97X-D,[35] which also includes dispersion correction. TDDFT calculations with the ωB97X-D functional have shown a very good performance for highly delocalised molecular systems.[36,37] Resolution of identity coupled cluster to the second order (CC2)[38] calculations were performed for the **G2** and **G2-2OH-C1** models with the def2-TZVP basis set. RI-CC2 results are in good agreement with the TDDFT calculations. A more detailed comparison of the results using different levels of theory can be found in the ESI.† Our discussion is based on the results obtained at the TDDFT-ωB97X-D/6-311+G(d) level of theory, unless otherwise specified.

The vertical excitations of the lowest 20 excited states were calculated using TDDFT. To be able to describe diffuse excited states, we consider a triplet zeta basis set including polarisation and diffuse functions, 6-311+G(d).[39] The ground state geometries of the functionalized **GO-QDs** were optimised at B3LYP/6-311+G(d) and ωB97X-D/6-311+G(d) levels of theory. The relaxation of the geometries in S_1 was done at TDDFT-B3LYP/6-311+G(d) and TDDFT-ωB97X-D/6-311+G(d) levels of theory.

The effect of vibrations on the broadening of the absorption spectra of **G2**, **G2-2OH-C1**, **G3** and **G3-2OH-C1** was considered using the nuclear ensemble approximation[40] as implemented in the Newton-X program.[41] This method considers that spectral broadening is obtained due to the contribution of an ensemble of structures generated from a Wigner distribution based on the harmonic frequencies. 20 excited states and 200 geometries were considered to perform these simulations. Further, to analyse the effect of solvent on the electronic spectrum of **G2**, the PCM method[42] was used considering cyclohexane as solvent.

The optical band gaps were calculated as the difference of energy between the ground and the first excited states.[43] The ionisation potentials were calculated as the energy difference between the cation and the neutral system. The atomic charges for the ground and the first excited states were obtained using the natural bond orbital (NBO) method.[44] DFT and TDDFT calculations were performed using the Gaussian program[45] and CC2 calculations using Turbomole.[46]

C. Results and discussion

Ionisation potentials

Similar to the interactions of organic molecules with metal surfaces in the application of self-assembled monolayers (SAMs),[47,48] **GO-QDs** can be covalently functionalized showing interesting behaviour on gold surfaces.[49] The design of efficient devices based on **GO-QDs** requires the understanding of the position of energy levels and their alignments with respect to the energy levels of molecules and metal contacts.[50] To provide

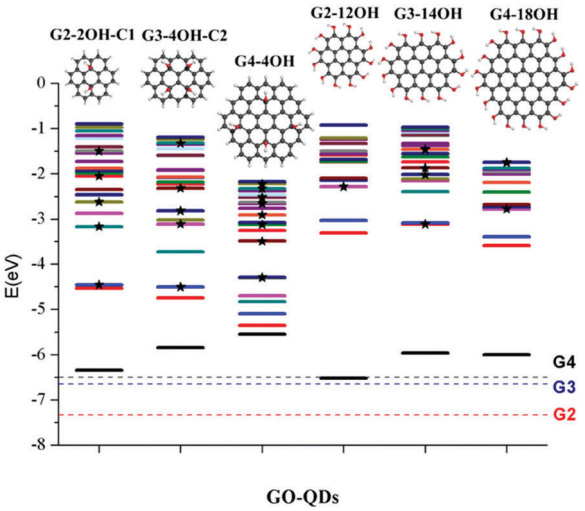

Fig. 2 20 lowest excited states for selected **GO-QDs** (TDDFT-ωB97X-D/6-311+G(d)). The electronic states were aligned with respect to vacuum, using the ionisation potentials calculated as the energy difference between the cation and the neutral **GO-QDs**. The energies of S_0 for the **GO-QDs** were shifted to the −IP value. The discontinuous lines show the −IP reference for the pristine QDs (**G2**: red, **G3**: blue, **G4**: black). The excited states with oscillator strengths larger than 0.1 are highlighted with stars.

an absolute reference for the electronic states of the considered **GO-QDs** models with respect to vacuum, the ionisation potentials were evaluated.

Fig. 2 illustrates the shift in the energy of the excited states of selected **GO-QDs**. Functionalisation with OH groups has an important effect on the first ionisation potentials (IP), which are smaller than the values of the corresponding pristine **G-QDs**. This effect can be understood considering the destabilisation of the occupied molecular levels because of the incorporation of atomic orbitals from electronegative atoms, which also has an effect on the optical band gaps which are smaller than in the corresponding pristine QDs.

In the series **G2**, **G3**, and **G4**, with the addition of aromatic rings the ionisation potentials decrease. In the case of **G2**, the calculated ionisation potential is 7.34 eV, in very good agreement with the experimental value of 7.29 eV.[51] The calculated IP for **G3** is 6.65 eV, which is also in good agreement with the experimental value of 6.71 eV.[51] The calculated ionisation potential for **G4** is 6.50 eV, which is only slightly shifted with respect to the value for **G3**.

These calculations show a strong effect of the position of the OH groups on the electronic properties and the optical gaps (Fig. 2). For **G2-2OH-C1**, the calculated IP is 6.34 eV, which is about 1 eV smaller than in **G2**. In the case of **G2-12OH** with edge functionalisation and a larger number of hydroxyl groups, the IP is reduced to 6.52 eV. For the **G3** and **G4** based **GO-QDs**, similar effects are observed. The IPs for **G3-4OH-C2** and **G3-12OH** are 5.84 and 5.96 eV respectively. In the case of **G4-18OH**, the ionisation potential is shifted to 6.00 eV, while the value for **G4-4OH** is 5.55 eV. In general, all examined electronic properties are more affected by functionalisation on the basal plane than by edge position substitutions. We analyse the reason for this behaviour in the next sections.

Tuning of optical gaps and fluorescence

Regardless of the position of the substituents, functionalisation with hydroxyl groups reduces the optical gap with respect to the values of the corresponding pristine QDs. In the case of **G2** and **G4** and the corresponding edge functionalised **GO-QDs** (**G2-12OH** and **G4-18OH**), the optical transitions and emission are not allowed by symmetry, but these transitions can show some intensity because of the geometry distortion caused by vibrations (the absorption and emission spectra of **G2** and **G3** are shown in Fig. 11 and 12). We have discussed the effect of substitutions on the oscillator strengths in the last section of the paper.

Fig. 3 shows the effect on the optical gaps and emission energy for all considered **G2** based QDs. The optical gap for coronene (**G2**) at the TDDFT-ωB97X-D/6-311+G(d) level of theory is 3.57 eV in very good agreement with the experimental value reported in cyclohexane which is 3.54 eV.[52] Our calculations using cyclohexane showed that the solvent does not affect the first absorption band (3.57 eV).

The **GO-QD** model with the smallest variation of optical gap values with respect to the pristine **G2** is **G2-12OH**, where all hydrogens were substituted by OH groups. The largest effect on the gaps is obtained when the **G2** is functionalised on the basal plane (**G2-2OH-C1**, **G2-2OH-C2**, **G2-4OH-C1**, **G2-4OH-C2** and **G2-12OH**). The relaxation of the geometry on the first excited state has a very small effect on the gap because the S_1 minima are only slightly distorted with respect to the Franck–Condon geometries. Emission energies show similar tendencies to the optical band gaps (Fig. 3). The larger Stokes shift (0.8 eV) is obtained for **G2-2OH-C2** and it is associated with reorientation of the hydroxyl groups.

HOMO, HOMO−1, LUMO and LUMO+1 frontier orbitals have the most important contributions to S_1. The features of these orbitals do not change significantly because of functionalisation (ESI†). The orbitals from the hydroxyl groups have a relatively small contribution to the frontier orbitals as can be

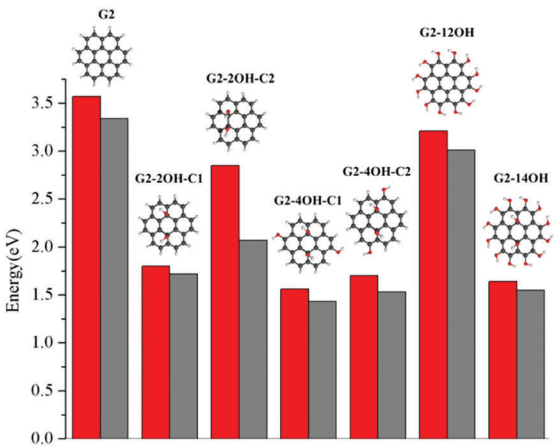

Fig. 3 S_1–S_0 optical gaps (in eV) calculated at the TDDFT-ωB97X-D/6-311+G(d) level of theory for the OH functionalised quantum dots based on pristine **G2**. Red bars correspond to the vertical excitation and grey bars to the fluorescence energy.

Table 1 The two most important electronic transitions contributing to S_1. H represents the HOMO orbitals and L represents the LUMO orbitals

GQs	Contributions (%) to S_1	
G2	H−1 → L 47.9%	H → L+1 47.9%
G2-2OH-C1	H−1 → L 78.0%	H → L+1 9.6%
G2-2OH-C2	H → L 85.1%	H−1 → L+1 6.0%
G2-4OH-C1	H−1 → L 51.7%	H → L 37.7%
G2-4OH-C2	H−1 → L 43.7%	H → L 42.0%
G2-12OH	H → L 34.0%	H−1 → L+1 34.0%
G2-14OH	H−1 → L 77.0%	H → L+1 20.0%

seen in the case of **G2-2OH-C1** and **G2-12OH**. For **G2**, the main electronic transitions involved in S_1 are HOMO → LUMO+1 (47.9%), HOMO−1 → LUMO (47.9%), HOMO → LUMO (2.0%) and HOMO−1 → LUMO+1 (2.0%). Functionalisation tunes the contributions of these transitions (Table 1).

For **G2-2OH-C1**, the most important transitions are HOMO−1 → LUMO (78.1%) and HOMO → LUMO+1 (9.6%). In the case of **G2-12OH**, the main electronic transitions are HOMO → LUMO (34.1%), HOMO−1 → LUMO+1 (34.1%), HOMO → LUMO+1 (13.6%) and HOMO−1 → LUMO (13.6%). In most cases, the first excited states show important contribution of at least two electronic transitions; consequently, the HOMO–LUMO analysis cannot provide a complete picture of these states. A detailed analysis of electron S_1–S_0 densities is discussed below in connection with the fluorescence mechanism.

Our calculations show that the tuning of the optical gap by basal plane functionalisation is mainly related to geometry distortion. The distortion from the planar geometry has an important effect on the localisation of the electron densities in S_0 and S_1. The analysis of the electron densities is in line with this interpretation and will be further analysed. The significant role of geometry distortion can be illustrated by substituting the OH groups by hydrogens in the **G2-2OH-C1** model. The obtained optical gap is 1.96 eV (1.94 eV without geometry relaxation). Considering that the optical gap for **G2-2OH-C1** is 1.80 eV, the most important effect of the basal plane functionalisation can be associated with geometry deformation. The effect of the functional group is minor.

Another important factor is the position of the functionalisation, which determines the number of aromatic rings deviated from the plane and less involved in the aromatic delocalisation. In general, **GO-QDs** with a larger number of distorted aromatic rings and more deviated from the plane have smaller optical gaps, more shifted with respect to the corresponding pristine QDs. Both factors are captured by the average angle θ (ESI†).

For **G2**, all positions in the (1,1) central unit are equivalent (see Fig. 7). In the case of **G2-2OH-C2** (θ = 17.9°), which has the same number of OH groups as **G2-2OH-C1** (θ = 20.7°), but a smaller deformation of the geometry, the reduction of the optical band gap (2.82 eV) with respect to **G2** is less significant. Considering the pattern of the functionalisation in **G2-2OH-C1**, five aromatic rings deviate significantly from the plane and four in the case of **G2-2OH-C2** (ESI†).

The effect of geometry distortion induced by edge functionalisation in elongated armchair graphene nanoflakes was examined by Cocchi *et al.* with important effects on the absorption properties.[53] Our edge functionalised **GO-QDs** do not show a significant geometry distortion because of the small size of the OH groups, which do not induce an important steric hindrance (the values of θ for **G2-12OH**, **G3-14OH** and **G4-18OH** are 1.3, 1.3 and 1.0 respectively, see ESI†). But some stabilisation in the system is detected due to the formation of hydrogen bonds.

In general, increasing the number of OH groups in the basal plane positions decreases the gap, but this effect strongly depends on the position of the functionalisation and correlates with the variation of the geometries. Substituting the edge hydrogens in **G2-4OH-C1** (θ = 21.2°) and **G2-4OH-C2** (θ = 20.9°) has a small effect on the gaps, with the values decreasing to 1.56 eV and 1.70 eV, respectively. The calculated optical band gap for **G2-14OH** (θ = 21.8°) is 1.64 eV. This model combines the functionalisation of **G2-2OH-C1** (optical gap: 1.80 eV) and the substitutions of **G2-12OH** (optical gap: 3.21 eV), which confirms that the most important effect on the optical band gap is the distortion of the geometry induced by the hydroxyl groups.

The effect of functionalisation on larger QDs is illustrated for **G3** and **G4**. While increasing the size of the aromatic system reduces the optical gaps, the effect of functionalization in larger QDs is similar to the observed for **G2**. The optical gaps are shifted to the red, with a larger effect of the basal plane functionalisation. The experimental absorption spectrum for **G3** in dichloromethane (dielectric constant = 8.93) shows the first band at 2.8 eV associated with the S_0–S_1 transition. The optical gap for **G3** is 3.15 eV (Fig. 4), which is about 0.4 eV smaller than in **G2**. The fluorescence excitation spectrum of **G3** in a supersonic beam showed the S_1–S_0 emission band (0–0 transition) at 2.66 eV,[54] which is in very good agreement with our calculated value of 2.79 eV. This transition showed a small

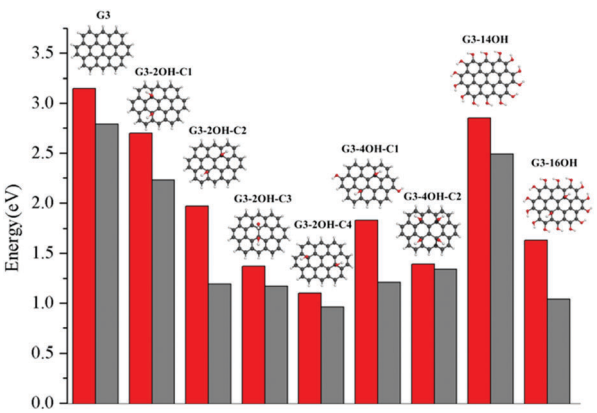

Fig. 4 S_1–S_0 optical gaps (in eV) calculated at the TDDFT-ωB97X-D/6-311+G(d) level of theory for the OH functionalised quantum dots based on pristine **G3**. Red bars correspond to the vertical excitation and grey bars to the fluorescence energy.

red shift (about 0.01 eV) in 1-methylnaphthalene solvent (dielectric constant = 2.7).[54]

G3 belongs to a lower symmetry group compared to **G2** and **G4**. Here, we consider the functionalisation of non-equivalent positions in **G3**. The largest shift from the **G3** optical gap is obtained for **G3-2OH-C4** (θ = 17.6°), with an optical gap of 1.10 eV, followed by **G3-2OH-C3** (1.37 eV, θ = 14.1°) (ESI†). While both **GO-QDs** show an important geometry distortion, there are other **G3** based **GO-QDs** with a more significant deviation from the plane. The reason for these small optical gaps is the functionalisation of positions with large electron–hole separation, which is analysed in the next section.

The effect of selective functionalisation of **G4** on the optical gaps is illustrated in Fig. 5. The calculated optical gap for **G4** is 2.68 eV. The largest effect on the gaps is obtained for **G4-22OH** (θ = 19.9°) with similar functionalisation to that in **G4-18OH** (θ = 9.8°) and **G4-4OH** (θ = 18.7°).

Controlling the fluorescence wavelength is very important for a wide range of applications. Small changes in the geometries in S_1 with respect to the Franck–Condon geometry were found. Consequently, the optical gaps and fluorescence energies are correlated (Fig. 3–5). All considered **GO-QDs** have their fluorescence wavelength shifted to the red with respect to the corresponding pristine **G-QDs**. The substitution of all the Franck–Condon geometry edge hydrogens shifted the fluorescence about 0.3 eV with respect to the pristine **G-QDs**. The oscillator strengths of these transitions are reported in the ESI.†

Fig. 6 shows the calculated **GO-QDs** with fluorescence in the visible region. The rest of the calculated **GO-QDs** have their emission wavelength in the infrared region or lower energy regions. If a significant shift is required, the basal carbons have to be functionalised. The combined effect of increasing the size of the **GO-QDs** and selective substitution can produce crossings between S_1 and S_0. This reduction of the gap is not favourable for applications because of competition between fluorescence and non-radiative mechanisms that are more likely to happen if the gap is small.

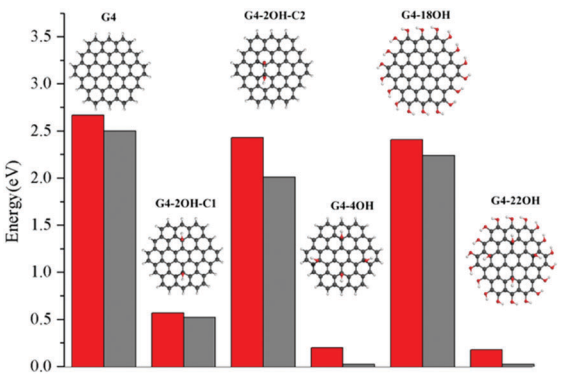

Fig. 5 S_1–S_0 optical gaps (in eV) calculated at the TDDFT-ωB97X-D/6-311+G(d) level of theory for the OH functionalised quantum dots based on pristine **G4**. Red bars correspond to the vertical excitation and grey bars to the fluorescence energy.

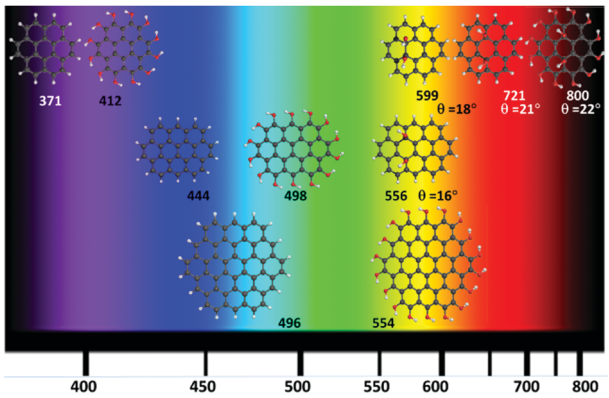

Fig. 6 Calculated **G-QDs** with fluorescence in the visible (nm) (TDDFT-ωB97X-D/6-311+G(d)).

Electron–hole separation

The study of the S_1–S_0 electron density differences shows the combined effect of all involved electronic transitions (Fig. 7–9). This analysis also provides information about the electron–hole separation induced by the electronic excitation. It has been proposed that fluorescence of **GO-QDs** can be associated with confinement of electrons within the sp^2 electron density clusters.[18] The plots of the electron density S_1–S_0 differences show localisation of electron density in specific regions of the **GO-QDs**. The mechanism of fluorescence of **GO-QDs** has also been associated with the CT to and from the functional groups during the electronic transition.

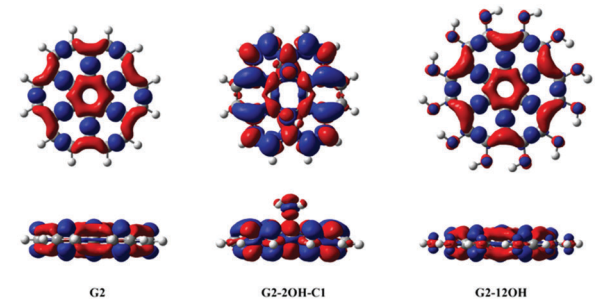

Fig. 7 Electron density differences (S_1–S_0) for **G2**, **G2-2OH-C1** and **G2-12OH**. At the bottom, the lateral views are shown. Positive regions are in red and negative regions are in blue. (Contours: 0.0004)

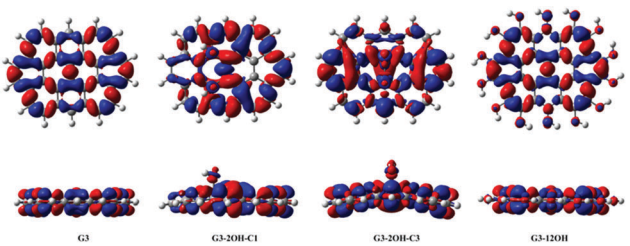

Fig. 8 Electron density differences (S_1–S_0) for **G3**, **G3-2OH-C1**, **G3-2OH-C3** and **G3-12OH**. At the bottom, the lateral views are shown. Positive regions are in red and negative regions are in blue. (Contours: 0.0004)

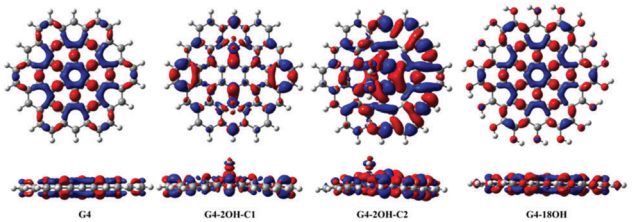

Fig. 9 Electron density differences (S_1–S_0) for **G4**, **G4-2OH-C1**, **G4-2OH-C2** and **G4-18OH**. At the bottom, the lateral views are shown. Positive regions are in red and negative regions are in blue. (Contours: 0.0004)

Basal plane functionalisation affects the geometries of the **GO-QDs**, which are not planar due to the change of hybridisation of the functionalised carbons from sp^2 to sp^3. At the same time, the contribution of the oxygen orbitals to electronic transitions destabilises the occupied molecular orbitals. The analysis of the electron densities of the excited state can aid in identifying which of these factors play a major role in the fluorescence mechanism. Our calculations show that the optical gap and emission are controlled by the creation of localised electron densities and that the role of CT to and from the hydroxyl groups is minor.

Functionalisation on the basal plane has an important effect on the electron–hole separation. The deformation of the geometry creates clusters with a large separation of the electron–hole. In contrast, functionalisation on the edge positions does not change significantly the distribution of the electron densities with respect to the pristine **G-QDs** (Fig. 7). This explains the minor effect of functionalisation on edge positions on the optical gaps and emission energies.

In the case of **G2** and **G2-12OH**, the excitation to S_1 increases the electron density on the central aromatic ring (1,1).[55] Only a small fraction of electron density from the hydroxyl groups is transferred to the aromatic system. To quantify the magnitude of the CT, we calculated the NBO charges in S_0 and S_1.

Our calculations show that in the case of **G2-2OH-C1**, the S_0–S_1 transition only increases the electron density of each hydroxyl oxygen about 0.013 e. For **G2-12OH**, a decrease of the electron density of about 0.004 e is found on each oxygen. In the case of **G2-14OH**, which combines edge and basal plane functionalisation, there is a small increase of the electron density on oxygen bonded to the basal C (0.011 e). The value of electron density on the hydroxyl groups depends on the position of the group. These calculations show that the CT from and to the hydroxyl groups does not play an important role in the first excited state and in the fluorescence of these **GO-QDs**.

The difference of S_1–S_0 electron densities shows a different pattern in **G3** when compared to **G2**. Excitation promotes electron density from three carbon centre π(C–C–C) to π(C–C) bonds (Fig. 8). In line with tuning of the optical gaps, functionalisation of the edge positions (**G3-12OH**) has a small effect on the electron densities, showing a similar symmetry and patterns as that obtained for **G3**. Our NBO calculations also show a small electron transfer between the hydroxyl groups and the QDs. In the case of **G3-2OH-C1**, the total electron transfer to the two hydroxyl groups is 0.03 e, which is larger than that obtained for similar **G2** based **GO-QDs** but still very small. The transfer from OH to the aromatic system in **G3-12OH** is also small, with an electron density of only 0.05 e transferred from the **G-QD** (about 0.004 per OH group).

To analyse the effect of the position of the functional group on the gaps, we consider the functionalisation of **G3** with two OH groups in the series **G3-2OH-C1**, **G3-2OH-C2**, **G3-2OH-C3**, and **G3-2OH-C4**. This series shows the important role of the position of the OH groups, which can be understood by analysing the electron–hole distribution in **G3**. **G3-2OH-C3** and **G3-2OH-C4** are obtained by functionalising carbon atoms with significant electron density (S_1–S_0) in the pristine **G3**. Consequently, they show a larger deviation of the optical gaps (Fig. 8).

In the series **G3-2OH-C1**, **G3-2OH-C2**, **G3-4OH-C1**, **G3-4OH-C2**, and **G3-16OH**, two OH groups are the functionalising positions with a node in the S_1–S_0 electron density. For these cases, a larger distortion of the geometry is related to larger deviation from the **G3** optical gap (ESI†). Increasing the number of hydroxyl groups from **G3-2OH-C2** to **G3-4OH-C1** has a minor effect on the optical gap (1.97 eV to 1.83 eV). This effect is more important for **G3-14OH**, where all hydrogens are substituted, but the main changes with respect to **G3** are due to the functionalisation of the basal plane positions similar to **G2-14OH**.

Our calculations show a small effect of the CT from or to the OH groups, with similar tendencies to that observed for **G2 GO-QDs**. In the case of functionalisation of the basal plane positions, a small electron transfer from the GDs can be found. For the **G3** based **G-QDs**, the maximum CT value was 0.02 e in the case of **G3-18OH**, to one of the OH bonded to a basal plane carbon. For the **G4** based **G-QDs**, the maximum CT is obtained for **G4-22OH** (0.03 e). The electron transfer from the OH on the edge positions is one order of magnitude smaller. These calculations show that the magnitude of CT from and to OH groups is very small, but there is a tendency of increasing the magnitude with the size of the **G-QDs**.

The comparison of the electron density (S_1–S_0) differences of **G2** and **G4** shows an inverse pattern (Fig. 9). The S_0–S_1 electron transition transfers electron density from the central C_6 aromatic unit (1,1) to the adjacent C–C bonds. That means that the hole has an important density on the central unit, in contrast to **G2** where the electron had a more significant density in the (1,1) central unit. There is a reordering of the frontier orbitals from **G2** to **G4**, where the HOMO and HOMO−1 occupied orbitals of **G2** resemble the LUMO and LUMO+1 of **G4** (ESI†).

G2 and **G4** belong to the same series of D_{6h} polycyclic hydrocarbons. Analysis of the ground state electron density using the natural density partitioning method shows that coronene (**G2**) has a layer of delocalised concentric pi-systems and circumcoronene (**G4**) has seven localised sextets, with only one Clar's structure (Fig. 10).[56] Clar's rule states that the Kekulé resonance structure with a larger number of disjoint aromatic sextets is the most important for the characterization of the properties of the ground state.[57]

This rule has implications for the electronic structure of the excited states because those structures with the least amount of

aromatic sextets will contribute more significantly to the excited states. Considering the topology of **G2**, the resonance structure with a larger number of disjoint sextets has 3 sextets in the outer region, while the resonance structure with one Kekulé structure contributes. Taking these ideas into account, Clar's rule beautifully explains the opposite behaviour of electron density differences observed for **G2** and **G4**.

Li *et al.* used quasiparticle calculations to analyse the effect of substitutions at one edge position of **G4** for different substituents, including OH.[26] The authors discussed the effect of orbital hybridisation and CT on the electronic structure and optical properties. Hybridisation was associated with a reduction of the gap, while CT was associated with opening of the gap. In the case of OH, significant hybridisation on the HOMO orbital was found, with a little effect on the LUMO orbital. The authors found a transfer of 0.93 e from the QD to the OH group based on atoms in molecules electron partition of the electron density. To compare with their results, we consider the QD as well (**G4-OH**) (ESI†).

In the ground state, we found a smaller electron transfer with NBO of about −0.2 e (−0.67 e for O and +0.47 e for H). Considering the differences in the electron densities between S_1 and S_0, only 0.002 e is transferred from the **G-QD** to the OH during the electron transition, which is in line with the small variation of the optical gap obtained for this **G-QD**. The optical band gap calculated at TDDFT-ωB97X-D/6-311+G(d) is 2.67 eV, which is only 0.01 eV shifted with respect to the **G4-QDs**. These calculations show that the CT from and to the OH does not have an important effect on the optical gap or the fluorescence mechanism.

Higher energy excited states

Fig. 2 shows that functionalisation has an important effect on the higher energy excited states. Regardless of their small intensities, some intermediate states could participate in the relaxation to the ground state. For example, S_2 might be involved in the de-excitation process of all considered **GO-QDs**. Non-adiabatic dynamics simulations showed the role of the intermediate states in the relaxation of perylene esters.[58] Here, we focus on the analysis of the effect of the brightest excited states, which have the most important contribution to the spectra. The effect of functionalisation on the absorption spectra is illustrated in the case of **G2-2OH-C1**.

The nuclear ensemble approximation was used to consider the effect of the vibrations on the absorption spectrum (Fig. 10).[40] **G2** has only two bright states in the region between 3.5 and 6.4 eV (first 20 excited states). These states are degenerate and correspond to S_3 and S_4 (4.71 eV and oscillator strength of 1.061, symmetry D_{6h}). The predicted band associated with the first bright state transition is red-shifted about 0.2 eV (4.5 eV). While considering the solvent the band is further red-shifted about 0.1 eV (4.4 eV), which shows a much better agreement with the experimental value of 4.10 eV.[52]

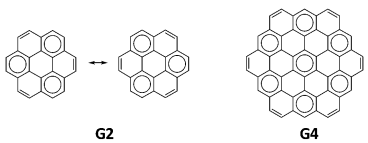

Fig. 10 Clar's structures for **G2** and **G4** showing the sextet in the ring (1,1) for **G4** and the external sextets for **G2**.

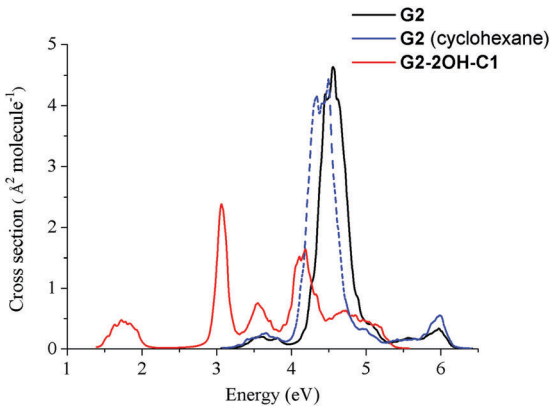

Fig. 11 Spectra of **G2** and **G2-2OH-C1** quantum dots calculated at the TDDFT-ωB97X-D/6-311+G(d) level of theory using the nuclear ensemble approximation.

The main effect of functionalisation on the spectra is the shift to the red, which is very important in the case of **G2-2OH-C1** because of the functionalisation of the basal plane carbons (Fig. 11). The first band, associated with the S_0–S_1 transition, is more intense than in the pristine **G2**. The intensities of the brightest states (S_3 and S_4) are distributed among several excited states in **G2-2OH-C1** and other models. In the series **G2**, **G2-2OH-C1**, **G2-2OH-C2**, **G2-4OH-C1**, and **G2-4OH-C2**, the energies of the first bright states are 4.71 (S_3, S_4), 3.25 (S_3), 3.11 (S_3), 3.25 (S_3), and 3.11 (S_3) respectively.

In general, substitutions on the basal plane positions lower the symmetry increasing the number of excited states with oscillator strengths larger than 0.1, but with smaller individual values (ESI†). Consequently, new features are found in the spectra (Fig. 11). For **G2-12OH**, where all edge positions are functionalised with hydroxyl groups (symmetry S_6), the energies of the brightest excited states are shifted to 4.23 eV (oscillator strength of 1.094) with similar stabilisation to that obtained for S_1.

In contrast to **G2** and **G4**, where S_1 has zero oscillator strength, for **G3** S_1 has an oscillator strength of 0.221 with an important contribution from the HOMO–LUMO transition (90%). The brightest excited state is S_6 (E = 4.32 eV, oscillator strength = 1.695) followed by S_7 (E = 4.52 eV, oscillator strength = 0.429) (ESI†). For S_6, the main electronic transitions are HOMO → LUMO+1 (48%) and HOMO−1 → LUMO (48%), while for S_7, the HOMO−1 → LUMO+2 transition has a contribution of 78%.

The functionalisation of the edge positions in **G3-14OH** shifted the energies of these states to $E(S_6)$ = 3.94 eV and $E(S_7)$ = 4.09 eV. The energy of the brightest excited states for basal plane functionalised **GO-QDs** is more affected. In the case of **G3-16OH** which combines functionalisation of the basal plane and the edge positions, the brightest excited state is S_{14} (E = 4.50 eV, oscillator strength = 0.713). There are many excited

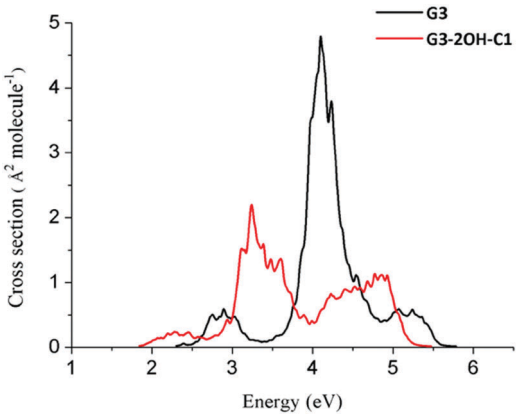

Fig. 12 Spectra of **G3** and **G3-2OH-C1** quantum dots calculated at the TDDFT-ωB97X-D/6-311+G(d) level of theory using the nuclear ensemble approximation.

states with significant oscillator strengths, such as S_5 (E = 3.34 eV, oscillator strength = 0.223), S_6 (E = 3.46 eV, oscillator strength = 0.323), S_8 (E = 3.88 eV, oscillator strength = 0.631), S_{10} (E = 4.15 eV, oscillator strength = 0.344), and S_{12} (E = 4.39 eV, oscillator strength = 0.272).

For **G3** based **GO-QDs**, the energy of the brightest excited states depends significantly on the position of the functionalisation. In general, the energy of the state is shifted to the red, but some substitution patterns show a small shift or even a shift to the blue. These differences are related to the reordering of the orbitals because of functionalisation and the creation of localised electron density clusters. In the case of **G3-2OH-C1**, **G3-2OH-C3**, and **G3-2OH-C4**, the energy of the brightest excited state is shifted to the red with energies of 3.71 eV (S_6), 3.12 eV (S_4) and 3.52 eV (S_6) respectively.

In the case of **G3-2OH-C2**, where two of the carbons are functionalised, the brightest states $E(S_8)$ = 4.23 eV (oscillator strength, 0.331), $E(S_9)$ = 4.37 eV (oscillator strength, 0.643), $E(S_{13})$ = 4.79 eV (oscillator strength, 0.376) and $E(S_{15})$ = 4.97 eV (oscillator strength, 0.638), which are close or blue-shifted with respect to the brightest states of **G3**.

If two hydroxyl groups are added to the edge positions to obtain **G3-4OH-C1**, the energy of these transitions is shifted to the red with $E(S_7)$ = 4.05 eV (oscillator strength, 0.407) and $E(S_9)$ = 4.24 eV (oscillator strength, 0.794). Adding the hydroxyl groups symmetrically in **G3-4OH-C2** produces a pattern similar to that observed for **G3-2OH-C1**, with a further redshift with $E(S_3)$ = 1.22 eV (oscillator strength, 1.219). These calculations show the important effect of the position of the functional groups on tuning the absorption properties of these **GO-QDs**. Similarly to the case of **G2**, functionalisation of **G3** to **G3-2OH-C1** shifted the whole spectrum to the red (Fig. 12). In contrast to **G2** the intensity of the first band decreased.

For **G4**, the brightest excited states are the degenerate S_3 and S_4 with an energy of 3.58 eV and an oscillator strength of 1.579. For **G4-18OH**, the energy of these states is shifted to 3.22 eV (oscillator strength = 1.657), which is similar to the shift for S_1. Functionalisation in the basal plane has a very strong effect on the energy levels of **G4** based QDs, as we have already discussed in the case of S_1. For the **GO-QDs** showing the most important shifts for S_1 (**G4-2OH-C1**, **G4-4OH** and **G4-22OH**) the brightest states shifted to the red.

In the case of **G4-2OH-C1**, the brightest excited state is S_8 with an energy of 2.94 eV. The addition of two hydroxyl groups to obtain **G4-4OH** shifted the energy to 2.89 eV. But several intermediate excited states showed significant intensity such as S_6 (1.26 eV, oscillator strength = 0.121), S_7 (2.06 eV, oscillator strength = 0.1087), S_9 (2.43 eV, 0.1098) and S_{11} (2.64 eV, oscillator strength = 0.387). The brightest excited state in **G4-22OH** is S_{13} with an energy of 2.58 eV (oscillator strength = 0.559). For **G4-2OH-C2**, in the low energy region, we can find S_3, S_4 and S_5 (3.19, 3.24 and 3.60 eV) with important oscillator strengths.

Conclusions

We modelled the effect of OH-functionalisation on the electronic structure of zigzag-edge **GO-QDs**. The effects of CT and geometry distortion on the optical gaps and fluorescence mechanism were considered. Unlike previous theoretical studies on **G-QDs** that considered the features of the frontier molecular orbitals, our analysis is based on the study of electron densities of the excited states.

Our calculations clearly show that the electronic properties of **GO-QDs** can be tuned by selective functionalisation with OH groups. Functionalisation with hydroxyl groups decreases the ionisation potentials of the **GO-QDs** with respect to the associated pristine **G-QDs**. Charge transfer from and to the hydroxyl groups does not play an important role in the fluorescence mechanism. More importantly, localization of sp^2 clusters due to the distortion of the geometry controls the S_1–S_0 transitions.

We predicted that the functionalisation of the positions with larger electron–hole separation in the pristine **G-QDs** affects largely the properties. Hydroxyl groups located on the basal plane have a remarkable effect on the properties, while substitutions on the edge plane affect the properties to a minor extent.

For functionalisation of positions with similar electron–hole separation in the pristine **G-QDs**, the optical gap strongly correlates with the distortion of the geometry induced by the substituent. The effect of increasing the functional groups depends on the position of the functionalisation and to what extent the geometry is deviated from the plane. Thus our analysis offers a strategy to tune the properties of **GO-QDs** based on the distortion of the geometry and the functionalisation of positions with large electron–hole separation in the pristine **G-QDs**.

Experiments have shown that reduction of oxidised **GO-QDs** blue shifted the fluorescence.[17,59] Our theoretical investigations show a similar tendency when the number of hydroxyl groups decreases from the functionalised **GO-QDs** to the corresponding pristine **G-QDs**.

Extensive functionalisation of basal plane positions should be damaging for several applications due to the associated reduction of the optical gap and fluorescence energy, which can

increase the probability of non-radiative crossings to the ground state. These results open up new opportunities for the design of OH functionalised **GO-QDs** for a wide range of applications.

Acknowledgements

The calculations were performed using the Queen Mary's MidPlus computational facilities, supported by QMUL Research-IT and funded by EPSRC grant EP/K000128/1 and NTU HPC clusters. RCO acknowledges the support from the School of Biological and Chemical Sciences at Queen Mary University of London.

References

1 K. P. Loh, Q. Bao, G. Eda and M. Chhowalla, *Nat. Chem.*, 2010, **2**, 1015–1024.
2 G. Eda, G. Fanchini and M. Chhowalla, *Nat. Nanotechnol.*, 2008, **3**, 270–274.
3 G. Eda and M. Chhowalla, *Adv. Mater.*, 2010, **22**, 2392–2415.
4 P. V. Kamat, *J. Phys. Chem. Lett.*, 2011, **2**, 242–251.
5 J. M. Yun, J. S. Yeo, J. Kim, H. G. Jeong, D. Y. Kim, Y. J. Noh, S. S. Kim, B. C. Ku and S. I. Na, *Adv. Mater.*, 2011, **23**, 4923–4928.
6 X. Zhu, Y. Zhu, S. Murali, M. D. Stoller and R. S. Ruoff, *ACS Nano*, 2011, 3333–3338.
7 J. William S. Hummers and R. E. Offeman, *J. Am. Chem. Soc.*, 1958, **80**, 1339.
8 T. Szab, O. Berkesi, P. Forg, K. Josepovits, Y. Sanakis, D. Petridis and I. Dkny, *Chem. Mater.*, 2006, 2740–2749.
9 A. Hunt, D. A. Dikin, E. Z. Kurmaev, T. D. Boyko, P. Bazylewski, G. S. Chang and A. Moewes, *Adv. Funct. Mater.*, 2012, **22**, 3950–3957.
10 M. Z. Hossain, J. E. Johns, K. H. Bevan, H. J. Karmel, Y. T. Liang, S. Yoshimoto, K. Mukai, T. Koitaya, J. Yoshinobu, M. Kawai, A. M. Lear, L. L. Kesmodel, S. L. Tait and M. C. Hersam, *Nat. Chem.*, 2012, **4**, 305–309.
11 A. Bagri, C. Mattevi, M. Acik, Y. J. Chabal, M. Chhowalla and V. B. Shenoy, *Nat. Chem.*, 2010, **2**, 581–587.
12 C. Y. Kong, W. L. Song, M. J. Meziani, K. N. Tackett, L. Cao, A. J. Farr, A. Anderson and Y. P. Sun, *J. Supercrit. Fluids*, 2012, **61**, 206–211.
13 G. Eda, Y. Y. Lin, C. Mattevi, H. Yamaguchi, H. A. Chen, I. S. Chen, C. W. Chen and M. Chhowalla, *Adv. Mater.*, 2010, **22**, 505–509.
14 W. Gao, L. B. Alemany, L. Ci and P. M. Ajayan, *Nat. Chem.*, 2009, **1**, 403–408.
15 S. Hu, *Chem. Rec.*, 2016, **16**, 219–230.
16 J.-A. Yan, L. Xian and M. Y. Chou, *Phys. Rev. Lett.*, 2009, **103**, 86802.
17 H. Zheng, Q. Wang, Y. Long, H. Zhang, X. Huang and R. Zhu, *Chem. Commun.*, 2011, **47**, 10650.
18 M. A. Sk, A. Ananthanarayanan, L. Huang, K. H. Lim and P. Chen, *J. Mater. Chem. C*, 2014, **2**, 6954.
19 M.-H. Jang, H. D. Ha, E.-S. Lee, F. Liu, Y.-H. Kim, T. S. Seo and Y.-H. Cho, *Small*, 2015, **11**, 3773–3781.
20 J. T. Robinson, S. M. Tabakman, Y. Liang, H. Wang, H. S. Casalongue, D. Vinh and H. Dai, *J. Am. Chem. Soc.*, 2011, **133**, 6825–6831.
21 S. Vempati and T. Uyar, *Phys. Chem. Chem. Phys.*, 2014, **16**, 21183–21203.
22 J. Peng, W. Gao, B. K. Gupta, Z. Liu, R. Romero-Aburto, L. Ge, L. Song, L. B. Alemany, X. Zhan, G. Gao, S. A. Vithayathil, B. A. Kaipparettu, A. A. Marti, T. Hayashi, J.-J. Zhu and P. M. Ajayan, *Nano Lett.*, 2012, **12**, 844–849.
23 S. S. R. K. C. Yamijala, M. Mukhopadhyay and S. K. Pati, *J. Phys. Chem. C*, 2015, **119**, 12079–12087.
24 M. Zhao, F. Yang, Y. Xue, D. Xiao and Y. Guo, *ChemPhysChem*, 2014, **15**, 157–164.
25 C. Cocchi, D. Prezzi, A. Ruini, M. J. Caldas and E. Molinari, *J. Phys. Chem. C*, 2012, **116**, 17328–17335.
26 Y. Li, H. Shu, X. Niu and J. Wang, *J. Phys. Chem. C*, 2015, **119**, 24950–24957.
27 C. Cocchi, D. Prezzi, A. Ruini, M. J. Caldas and E. Molinari, *J. Phys. Chem. C*, 2012, **116**, 17328–17335.
28 M. Zhao, F. Yang, Y. Xue, D. Xiao and Y. Guo, *ChemPhysChem*, 2014, **15**, 950–957.
29 I. A. Popov and A. I. Boldyrev, *Eur. J. Org. Chem.*, 2012, 3485–3491.
30 P. Johari and V. B. Shenoy, *ACS Nano*, 2011, **5**, 7640–7647.
31 C. Cocchi, D. Prezzi, A. Ruini, M. J. Caldas and E. Molinari, *J. Phys. Chem. Lett.*, 2011, **2**, 1315–1319.
32 S. S. R. K. C. Yamijala, M. Mukhopadhyay and S. K. Pati, *J. Phys. Chem. C*, 2015, **119**, 12079–12087.
33 M. E. Casida, *THEOCHEM*, 2009, **914**, 3–18.
34 A. D. Becke, *J. Chem. Phys.*, 1993, **98**, 5648.
35 J.-D. Chai and M. Head-Gordon, *Phys. Chem. Chem. Phys.*, 2008, **10**, 6615–6620.
36 K. Sen, R. Crespo-Otero, W. Thiel and M. Barbatti, *Comput. Theor. Chem.*, 2014, **1040–1041**, 237–242.
37 K. Sen, R. Crespo-Otero, O. Weingart, W. Thiel and M. Barbatti, *J. Chem. Theory Comput.*, 2013, **9**, 533–542.
38 C. Hättig and A. Köhn, *J. Chem. Phys.*, 2002, **117**, 6939.
39 R. Krishnan, J. S. Binkley, R. Seeger and J. A. Pople, *J. Chem. Phys.*, 1980, **72**, 650.
40 R. Crespo-Otero and M. Barbatti, *Theor. Chem. Acc.*, 2012, **131**, 1237.
41 M. Barbatti, G. Granucci, M. Ruckenbauer, F. Plasser, R. Crespo-Otero, J. Pittner, M. Persico and H. Lischka, *NEWTON-X: a package for Newtonian dynamics close to the crossing seam*, 2013, http://www.newtonx.org.
42 J. Tomasi, B. Mennucci and R. Cammi, *Chem. Rev.*, 2005, **105**, 2999–3093.
43 J.-L. Bredas, *Mater. Horiz.*, 2014, **1**, 17–19.
44 A. E. Reed, R. B. Weinstock and F. Weinhold, *J. Chem. Phys.*, 1985, **83**, 735.
45 M. J. Frisch, G. W. Trucks, H. B. Schlegel, G. E. Scuseria, M. A. Robb, J. R. Cheeseman, G. Scalmani, V. Barone, B. Mennucci, G. A. Petersson, H. Nakatsuji, M. Caricato, X. Li, H. P. Hratchian, A. F. Izmaylov, J. Bloino, G. Zheng, J. L. Sonnenberg, M. Hada, M. Ehara, K. Toyota, R. Fukuda, J. Hasegawa, M. Ishida, T. Nakajima, Y. Honda, O. Kitao,

H. Nakai, T. Vreven, J. A. Montgomery, Jr., J. E. Peralta, F. Ogliaro, M. Bearpark, J. J. Heyd, E. Brothers, K. N. Kudin, V. N. Staroverov, T. Keith, R. Kobayashi, J. Normand, K. Raghavachari, A. Rendell, J. C. Burant, S. S. Iyengar, J. Tomasi, M. Cossi, N. Rega, J. M. Millam, M. Klene, J. E. Knox, J. B. Cross, V. Bakken, C. Adamo, J. Jaramillo, R. Gomperts, R. E. Stratmann, O. Yazyev, A. J. Austin, R. Cammi, C. Pomelli, J. W. Ochterski, R. L. Martin, K. Morokuma, V. G. Zakrzewski, G. A. Voth, P. Salvador, J. J. Dannenberg, S. Dapprich, A. D. Daniels, O. Farkas, J. B. Foresman, J. V. Ortiz, J. Cioslowski and D. J. Fox, *Gaussian 09, Revision C.01*, Gaussian, Inc., Wallingford CT, 2010.

46 R. Ahlrichs, M. Bär, M. Häser, H. Horn and C. Kölmel, *Chem. Phys. Lett.*, 1989, **162**, 165–169.

47 C. M. Crudden, J. H. Horton, I. I. Ebralidze, O. V Zenkina, A. B. McLean, B. Drevniok, Z. She, H.-B. Kraatz, N. J. Mosey, T. Seki, E. C. Keske, J. D. Leake, A. Rousina-Webb and G. Wu, *Nat. Chem.*, 2014, **6**, 409–414.

48 K. R. Geethalakshmi, X. Yang, Q. Sun, T. Y. Ng and D. Wang, *RSC Adv.*, 2015, **5**, 88625–88635.

49 A. B. Shivanandareddy, M. Kumar, V. Lakshminarayanan and S. Kumar, *RSC Adv.*, 2015, **5**, 47692–47700.

50 P. V. C. Medeiros, G. K. Gueorguiev and S. Stafström, *Phys. Rev. B: Condens. Matter Mater. Phys.*, 2012, **85**, 205423.

51 E. Clar, J. M. Robertson, R. Schloegl and W. Schmidt, *J. Am. Chem. Soc.*, 1981, **103**, 1320–1328.

52 R. Rieger, M. Kastler, V. Enkelmann and K. Müllen, *Chem. – Eur. J.*, 2008, **14**, 6322–6325.

53 C. Cocchi, D. Prezzi, A. Ruini, M. J. Caldas and E. Molinari, *J. Phys. Chem. C*, 2012, **116**, 17328–17335.

54 A. Amirav, *J. Chem. Phys.*, 1981, **74**, 3745.

55 I. Gutman, S. J. Cyvin and V. Ivanov-Petrović, *Z. Naturforsch., A: Phys. Sci.*, 1998, **53**, 699–703.

56 I. A. Popov and A. I. Boldyrev, *Eur. J. Org. Chem.*, 2012, 3485–3491.

57 M. Solà, *Front. Chem.*, 2013, **1**, 22.

58 J. Vollbrecht, C. Wiebeler, A. Neuba, H. Bock, S. Schumacher and H. Kitzerow, *J. Phys. Chem. C*, 2016, **120**, 7839–7848.

59 C.-T. Chien, S.-S. Li, W.-J. Lai, Y.-C. Yeh, H.-A. Chen, I.-S. Chen, L.-C. Chen, K.-H. Chen, T. Nemoto, S. Isoda, M. Chen, T. Fujita, G. Eda, H. Yamaguchi, M. Chhowalla and C.-W. Chen, *Angew. Chem., Int. Ed.*, 2012, **51**, 6662–6666.

